Mechanical and fracturing characteristics of defected cement mortar samples under biaxial confinements

Pengxuan Ji
Monash University, Melbourne, Australia

Qianbing Zhang
Monash University, Melbourne, Australia

Gisela Viegas
Newcrest Mining Limited, Melbourne, Australia

ABSTRACT: In this study, quasi-static biaxial compression tests are conducted on rock-like cement mortar materials to examine the effect of shape, orientation, and interaction of pre-existing defects representing the rock mass with fissures created by nature or hydrofracturing. The mechanical and fracturing characteristics are investigated by stress-strain response, acoustic emission, digital image correlation and synchrotron X-ray computed tomography techniques. Results show the biaxial compression strength (σ_{BCS}) increases with confinement and restricts the development of cracks compared to uniaxial tests. In terms of hole samples, the confinement squeezes the tensile stress concentration area at the crown and invert of the hole. The orientation of the flaw impacts the failure characteristics and σ_{BCS} reaches its lowest value when the inclination angle is 45 degrees. The proposed integrated analysis framework is proven to be feasible for samples with more complicated geometry and the findings would benefit underground civil and resource-related projects.

Keywords: Biaxial compression, Cement mortar, Pre-existing defect, Fracturing characteristic, Integrated analysis framework, Analytical solution.

1 INTRODUCTION

Rock mass in underground excavation often contains various types of pre-existing discontinuities affecting rock stability (Bobet & Einstein 1998). Additionally, fractures are sometimes artificially created by hydrofracturing, which could lead to the reactivation of pre-existing faults (Goodfellow et al. 2015), and the associated release of tectonic stresses (Maxwell & Rutledge 2013). Thus, a deep understanding of the failure behavior of the rock mass with pre-existing natural or artificial defects is important in mining and tunneling engineering. Seismic activity provides a powerful measure for geophysical surveys, which shares similar physical processes at several scales, although at different frequency bands and energy release levels (Goodfellow & Young 2014). The field-scale microseismic (MS) monitoring has been used to indicate fracturing activities in underground rocks as a passive seismic technique (Li et al. 2020). However, due to the limitations such as complex noise sources and various unknown influence factors, the lab-scale experiment is preferred for an accurate study of seismic mechanisms under controlled conditions, where the acoustic emission (AE)

characteristics could be obtained. To better interpret the fracturing characteristics, the integrated analysis framework including digital image correlation (DIC) and synchrotron-based computed tomography (CT) for surface strain field and internal patterns respectively is applied. Besides, existing studies mainly investigate the effects of fabricating defects under uniaxial loading conditions, but the stress state on the surface of the rock mass changes from triaxial loading to biaxial loading after excavation (Cai & Kaiser 2014; Liu et al. 2019). Although real rocks can realistically reveal the fracturing characteristic of engineering rock, rock-like materials are widely used in experiments for easier preparation of multiple pre-existing defects and avoidance of artificial processing damages (Lee et al. 2017). Cement mortar is proven to be a good substitute for field samples (Cao et al. 2015).

In this study, quasi-static biaxial compression tests are conducted on cement mortar and sandstone samples. Real-time crack growth from microscopic to macroscopic scale is analyzed in detail by AE and DIC techniques, and the internal failure pattern is reconstructed by CT technique.

2 EXPERIMENTAL PROCEDURES

2.1 Specimen Preparation

Rock-like cement mortar material is used to prepare specimens. The cement mortar sample fabricated in this study is composed of general-purpose cement, fine sand and water in a mass ratio of 2:4:1. The mixed mortar is poured into molds. Then they are kept in a water tank for curing for 7 days. The prepared specimens are polished into the size of 100 mm, 50 mm and 100 mm in length, width and height, respectively, succeeded by speckle pattern spraying for DIC analysis. Four types of samples are prepared, which are intact specimens, hole specimens, single-flawed specimens and specimens containing intersected hole and single flaw. The flaw and hole are fabricated by presetting a steel sheet and a pipe into the mold. The preparation procedure is displayed in Figure 1.

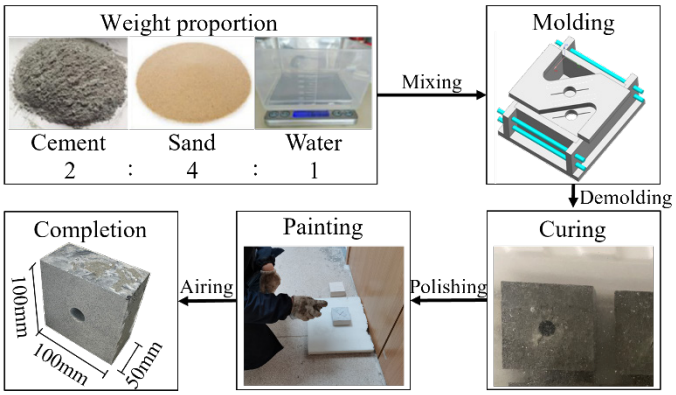

Figure 1. Preparation process of cement mortar samples with pre-existing defects.

2.2 Loading and data acquisition system

The experimental and measurement techniques are shown in Figure 2. To provide controllable and stable lateral confined pressure (σ_3), the loading apparatus is newly designed to be installed on the Instron 600 machine for quasi-static tests. To monitor the acoustic signal generated during the test, the high-speed AE monitoring system composed of a data acquisition (DAQ) system and Lead Zirconate Titanate (PZT) sensors is used. The real-time full-field deformation and strain field are quantitatively measured by the DIC method combined with two high-speed cameras (Phantom V2511, up to 1 million frames per second). The results in colour demonstrate the distribution of strain fields in X direction (ε_{XX}). X-ray CT technique is powerful to capture the internal structures of post-failure samples. Owing to the diversity of material density, X-ray attenuation varies, represented by the brightness contrasts over different phases in grayscale images (Mees et al. 2003). The CT images are obtained using IMBL in Australian Synchrotron and further reconstructed by Avizo 9.5.

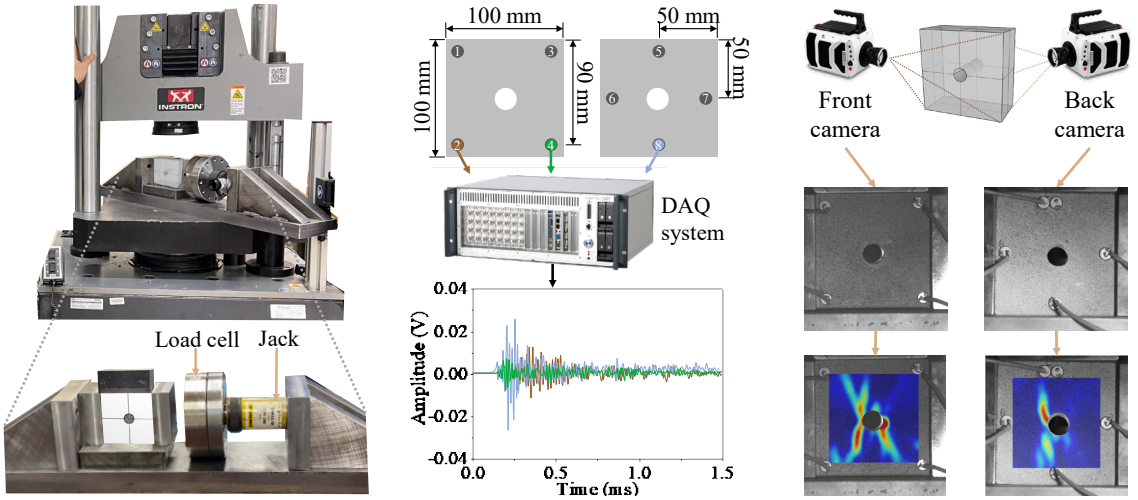

(a) Loading system (b) AE acquisition system (c) High-speed cameras & DIC

Figure 2. Experimental setup and integrated analysis framework.

3 EXPERIMENTAL RESULTS

3.1 Intact and hole samples

The effect of confinement on intact and hole samples is shown in Figure 3(a), where the AE activity is included to reveal crack levels. The biaxial compression strength (σ_{BCS}) increases with the rise of confined pressure, for confinement restricts the lateral deformation significantly. Figure 3(b) shows that the intact specimen exhibits tensile-dominant failure in the uniaxial test. In terms of the biaxial test, the lateral confinement restricts the development of cracks, so it is hard to capture an obvious rupture on the surface. When σ_3 is 10 MPa, there is an extra sudden rise shown in AE activities during the loading, indicating a fracture occurred inside the specimen before the final failure.

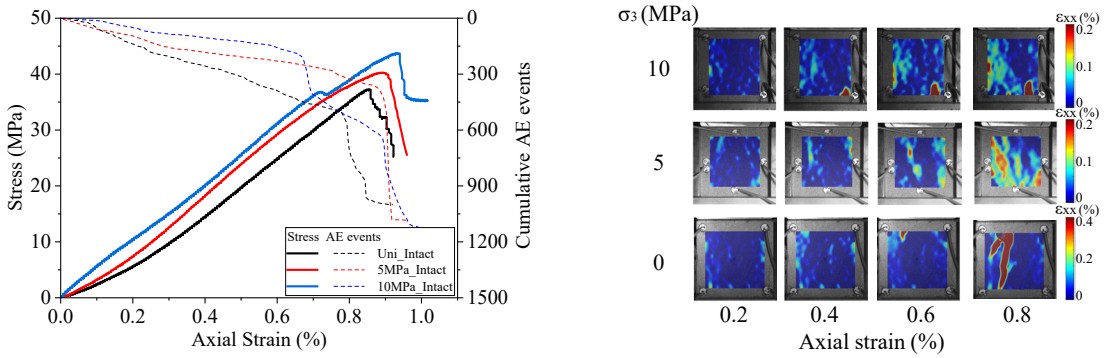

(a) Stress and AE event curves of intact samples (b) Strain field of intact samples

Figure 3. Experimental results of intact samples under different confinements.

Figure 4 illustrates the analytical solution for a single cavern subjected to the biaxial field stress p and κp according to the equations below, giving the stresses on the excavation boundary (Brady & Brown 2004). The variation of tangential stress ($\sigma_{\theta\theta}$) with the observation angle (θ) and the ratio of vertical stress and lateral stress (κ) is plotted based on the theoretical analysis, when p is 5 MPa.

$$\sigma_{\theta\theta} = p[(1+\kappa) - 2(1-\kappa)cos2\theta] \quad \sigma_{rr} = 0 \quad \sigma_{r\theta} = 0 \tag{1}$$

where σ_{rr} is the radial stress, and $\sigma_{r\theta}$ is the shear stress.

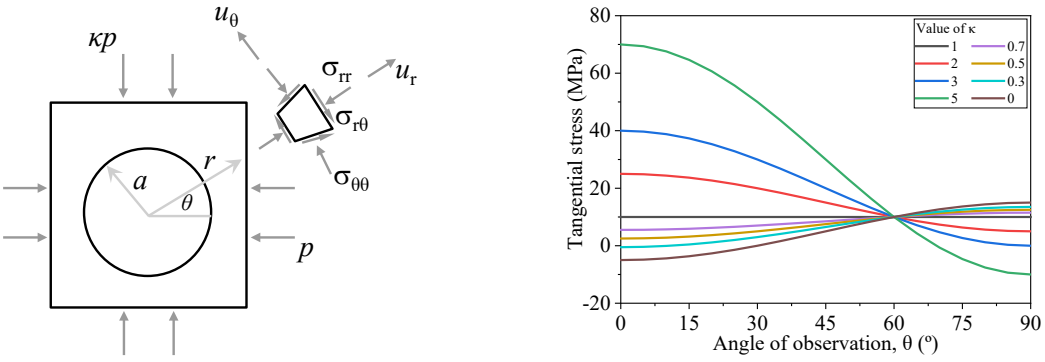

(a) The hole specimen under biaxial loading (b) Tangential stress of hole specimens

Figure 4. The analytical solution to the hole specimen (modified after Brady & Brown 2004).

For a given κ larger than 1, the observation angle θ greatly influences the tangential stress, and the lowest is always obtained at 90°. This indicates that tensile cracks could initiate at the crown and invert of a cavern. The strain field result in Figure 5(b) calculated by the DIC method shows that strain localizations are originally observed roughly at these two positions indicating the onset of crack growth. The result corresponds to the theory, but it is not completely accurate. This is because κ is a constant in theoretical analysis, instead of a variable dependent on the loading rate in tests and excavations. These initiated tensile cracks extend limitedly. With the increase of σ_3, they tend to become shorter or disappear, for the tensile stress concentration area is shrunk. Then, the hole shows a trend to deform to an elliptic shape and the shear cracks occur at two sides close to the compressive stress concentration area which will then be released and transferred to the tip region of new cracks. Finally, the propagation and coalescence of far field cracks result in failure. For confined samples, cracks extend along the diagonal direction and pass through the hole, and lead to X-type shear failure.

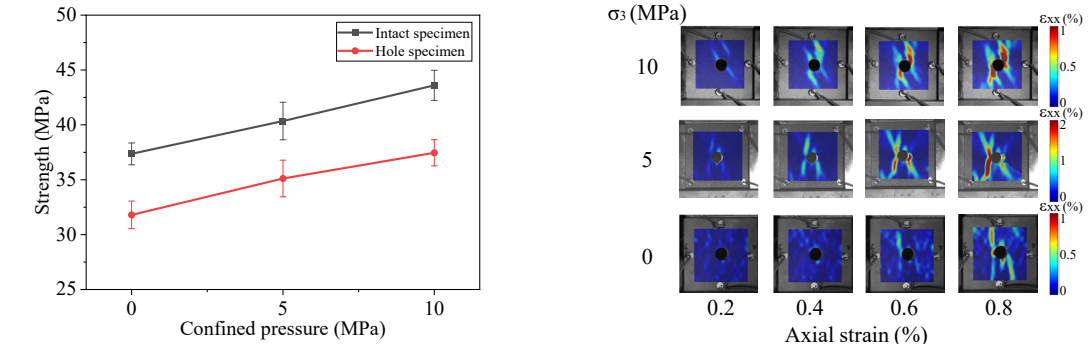

(a) Strength of intact samples and hole samples (b) Strain field of hole samples

Figure 5. Experimental results of hole samples under different confinements.

3.2 *Single-flawed samples*

The theoretical analysis of single-flawed samples under biaxial loading is based on the equations below (Eftis & Subramonian 1978). The variation of the initiation angle θ_0 with pre-existing flaw inclined angle α is plotted as shown in Figure 6 founded on the analytical solution, when p is 5 MPa.

$$1.75[B_1(3\cos\theta_0 - 1) + 3B_2\sin\theta_0] - 4B_3\sin\frac{\theta_0}{2}\cos\theta_0 = 0 \tag{2}$$

$$B_1 = -\frac{3}{2}(1-\kappa)\sin 2\alpha \quad B_2 = \kappa + (1-\kappa)\cos^2\alpha \quad B_3 = -(1-\kappa)\cos 2\alpha$$

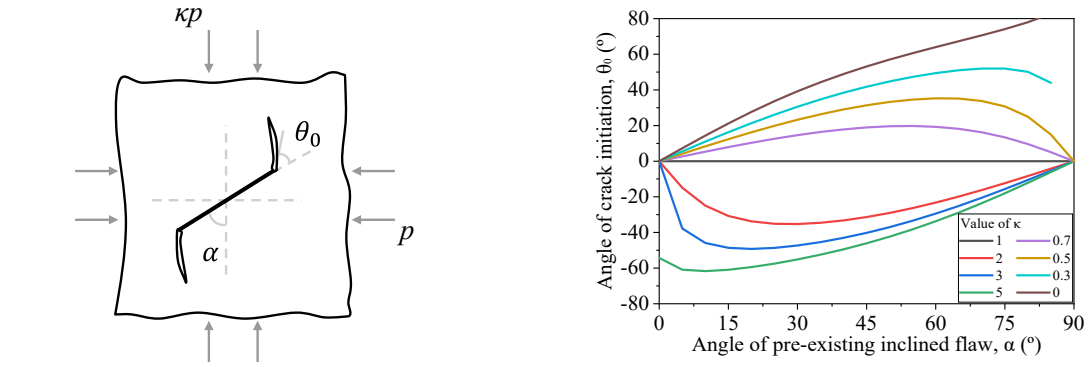

(a) The flawed specimen under biaxial loading (b) Crack initiation angle of flawed specimens

Figure 6. The analytical solution to the single-flawed specimen (modified after Eftis & Subramonian 1978).

The effect of flaw orientation on strength and a part of strain field results are shown in Figure 7. With the increase of α, the strength slightly increases before dropping markedly to hit the lowest value at 45°, and then rises limitedly. During loading, the confinement restricts the tensile concentration area. The anti-wing cracks initiate from the tips and propagate downwards. However, the increase of α negatively affects the shearing on the flaw surface, and cracks gradually develop away from the flaw, meaning a decreasing trend of θ_0. This is consistent with the analytical solution, where for a given κ larger than 1, there is a negative correlation between θ_0 and α, when α ranges from 15° to 75°.

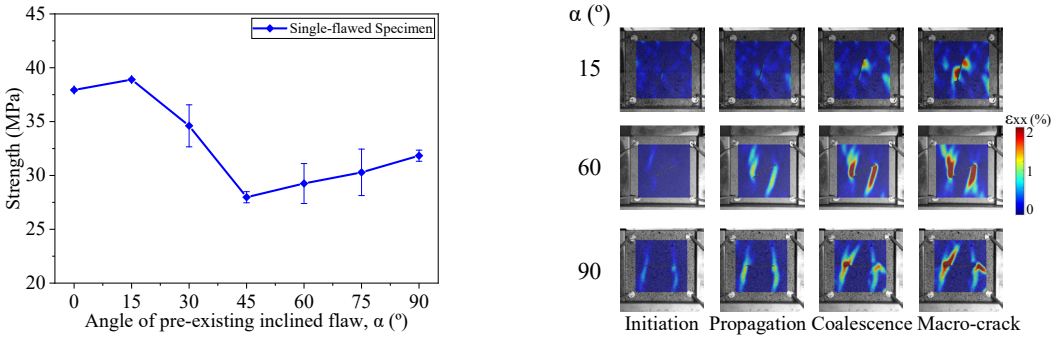

(a) The effect of flaw orientation on strength (b) Strain field at different moments

Figure 7. Experimental results of single-flawed samples.

3.3 Integrated analysis of the effect of interaction of defects

The photo, strain field and fracture volume rendering of a post-failure sample are shown in Figure 8, together with AE events, where the color represents the temporal distribution of micro-cracks, and the size stands for the scale of the location magnitude. Technically, the AE activities could not be located as precisely as the surface behaviors. Thus, the integrated framework for cross-validation is applied, where the failure pattern could be revealed both internally and externally. The interaction of defects decreases the tensile concentration area at the upper and lower ends of the hole, but the shear stress would concentrate at two sides of the cavern and coalesce with the anti-wing cracks.

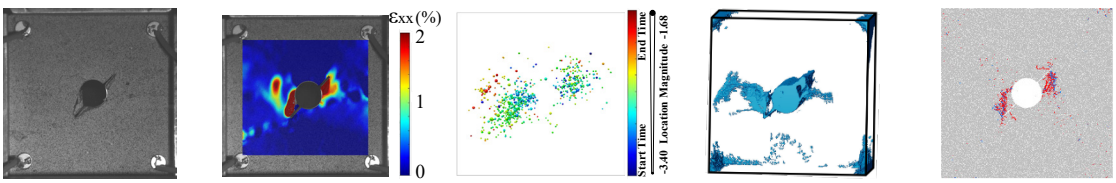

(a) Image (b) Strain field (c) AE events (d) X-ray CT (e) DEM model

Figure 8. Cross-validation on the sample with pre-existing hole and flaw.

CONCLUSION

In this study, the biaxial compression tests of defected cement mortar specimens are carried out, and the mechanical and fracturing characteristics are explored through the correlation among stress-strain response, AE activities, strain field and CT reconstruction model. The results reveal the effect of confinement increases the sample strength and restricts the development of cracks compared to uniaxial tests with tensile-dominant failure. The benchmark verification of hole specimens shows that the cracks initiate from the top and bottom of the hole, while that of single-flawed specimens displays that the cracks originate from the tips of the flaw. They follow the analytical solution to some extent, but it is not completely accurate due to the variability of κ in the tests and engineering constructions. The integrated analysis framework has been proven to be feasible to investigate accurate fracturing behaviors of samples with more complicated factors of pre-existing fissures representing the preconditioned rock geometry. The interaction of a hole and a flaw changes the stress distribution, shrinking the tensile concentration area greatly at the crown and invert of the hole.

ACKNOWLEDGEMENT

The first author would like to acknowledge the Monash Graduate Scholarship. The authors would also like to acknowledge the support from Newcrest Mining Limited and Australian Synchrotron (Project No.: 18986).

REFERENCES

Bobet, A. & Einstein, H.H. 1998. Fracture coalescence in rock-type materials under uniaxial and biaxial compression. *International Journal of Rock Mechanics and Mining Sciences*, *35*(7), 863–888. DOI: 10.1016/S0148-9062(98)00005-9

Brady, B.H.G. & Brown, E.T. 2004. *Rock mechanics: For underground mining* (3rd ed). Kluwer Academic Publishers.

Cai, M. & Kaiser, P.K. 2014. In-situ Rock Spalling Strength near Excavation Boundaries. *Rock Mechanics and Rock Engineering*, *47*(2), 659–675. DOI: 10.1007/s00603-013-0437-0

Cao, P., Liu, T., Pu, C. & Lin, H. 2015. Crack propagation and coalescence of brittle rock-like specimens with pre-existing cracks in compression. *Engineering Geology*, *187*, 113–121. DOI: 10.1016/j.enggeo.2014.12.010

Eftis, J. & Subramonian, N. 1978. The inclined crack under biaxial load. *Engineering Fracture Mechanics*, *10*(1), 43–67. DOI: 10.1016/0013-7944(78)90049-8

Goodfellow, S.D. & Young, R.P. 2014. A laboratory acoustic emission experiment under in situ conditions. *Geophysical Research Letters*, *41*(10), 3422–3430. DOI: 10.1002/2014GL059965

Goodfellow, S.D., Nasseri, M.H.B., Maxwell, S.C. & Young, R.P. 2015. Hydraulic fracture energy budget: Insights from the laboratory. *Geophysical Research Letters*, *42*(9), 3179–3187. DOI: 10.1002/2015GL063093

Lee, J., Ha, Y.D. & Hong, J.-W 2017. Crack coalescence morphology in rock-like material under compression. *International Journal of Fracture*, *203*(1–2), 211–236. DOI: 10.1007/s10704-016-0138-2

Li, L., Tan, J., Schwarz, B., Staněk, F., Poiata, N., Shi, P., Diekmann, L., Eisner, L. & Gajewski, D. 2020. Recent Advances and Challenges of Waveform-Based Seismic Location Methods at Multiple Scales. *Reviews of Geophysics*, *58*(1). DOI: 10.1029/2019RG000667

Liu, X., Liu, Q., Liu, B., Zhu, Y. & Zhang, P. 2019. Failure Behavior for Rocklike Material with Cross Crack under Biaxial Compression. *Journal of Materials in Civil Engineering*, *31*(2), 06018025. DOI: 10.1061/(ASCE)MT.1943-5533.0002540

Maxwell, S. & Rutledge, J. 2013. Deformation investigations of induced seismicity during hydraulic fracturing. *SEG Technical Program Expanded Abstracts 2013*, 4521–4525. DOI: 10.1190/segam2013-1415.1

Mees, F., Swennen, R., Geet, M.V. & Jacobs, P. 2003. Applications of X-ray computed tomography in the geosciences. *Geological Society, London, Special Publications*, *215*(1), 1–6. DOI: 10.1144/GSL.SP.2003.215.01.01